Contactless Permanent Magnet Temperature Detection of PMSM based on the Input DC Power of the Auxiliary Inverter

Ryo Hamba[1], Keisuke Kusaka[1]*, Yoshihisa Hojo[2]
1 Dept. of Electrical, Electronics and Information Engineering, Nagaoka University of Technology, Nagaoka, Japan
2 Development Center, Toyo Denki Seizo K.K., Yokohama, Japan
* kusaka@vos.nagaokaut.ac.jp

***Abstract*— Managing magnet temperature is essential for enhancing the accuracy and reliability of torque control in permanent magnet synchronous motors (PMSMs). This paper proposes a temperature detection method for PMSM magnets that employs wireless power transfer combined with a thermistor. The method estimates the thermistor temperature from the DC input power of the detection circuit. The influence of winding resistance variation on temperature-detection accuracy was analyzed through simulation. Results indicate that choosing a thermistor resistance close to the derived optimal value enhances robustness and minimizes detection errors. Experimental results demonstrate that the input power decreases monotonically as the thermistor temperature increases, and that the proposed method achieves a detection accuracy of ±4°C.**

Keywords—Permanent Magnet Synchronous Motor, Temperature Detection, Wireless Power Transfer.

I. INTRODUCTION

Permanent magnet synchronous motors (PMSMs) offer high efficiency and high torque density. Therefore, they are widely used in applications such as electric vehicles, railway traction systems, household appliances, and testing machines. In the permanent magnets used in the rotor of a PMSM, eddy currents are induced by spatial harmonics and carrier harmonics originating from the inverter, resulting in heat generation [1–3]. The resulting temperature rise of the permanent magnets can cause demagnetization. For instance, in neodymium magnets (NdFeB magnets), the residual flux density decreases by approximately 0.13% for every 1°C increase in temperature [4]. Because the torque of a PMSM depends on the magnetic flux produced by the permanent magnets, the temperature rise of the magnets affects the motor torque [5–6]. In addition, the coercivity decreases by approximately 1.77% for every 1°C increase in temperature [4]. As a result, excessive heating of the permanent magnets may cause irreversible demagnetization. This permanently decreases the magnetic force and may prevent the motor from delivering the required torque output.

To address these issues, motor protection is generally achieved by limiting the continuous operating time or output torque. However, because the actual magnet temperature depends on the ambient temperature of the motor and its previous operating conditions, when the exact magnet temperature is unknown, the protection system must be designed based on worst-case assumptions. As a result, excessively large safety margins must be incorporated into the protection design, which leads to underutilization of the motor's full performance potential. From this perspective, techniques for measuring or estimating magnet temperature are required to improve the reliability and torque-control accuracy of PMSMs and to reduce excessive safety margins in protection design.

A traditional method for determining magnet temperature involves coupling a temperature sensor with a slip ring [7]. In this method, the magnet temperature data from the rotor are transmitted to the outside through the slip ring. However, contact between the ring and the brush leads to poor durability and maintainability, resulting in reliability issues. As an alternative approach without physical contacts, such as slip rings, methods have also been proposed in which temperature data measured by a temperature sensor are transmitted via wireless communication [8–10]. In reference [8], the measurement method with an accuracy of ±1.5°C was reported. However, such methods require additional components on the rotating part, such as a battery, and therefore necessitate periodic maintenance. As a method that does not require additional components on the rotor side, non-contact temperature measurement using infrared thermographic cameras or thermometers has also been employed [11–17]. However, this approach can only measure the surface temperature of the target object. While it is suitable for measuring temperature at the rotor end, it is not appropriate for gauging the temperature near the rotor's center. The high cost of infrared cameras also remains an issue.

Temperature estimation methods based on either thermal or electrical models have been proposed. Thermal-model-based methods [11], [18–24] estimate the magnet temperature by modeling the heat-transfer paths within the PMSM as a thermal circuit. In reference [11], magnet temperature estimation with an error of up to 3°C was demonstrated. However, the parameters of the thermal circuit are generally sensitive to changes in the surrounding environment and cooling system, and the estimation accuracy may deteriorate when operating conditions differ from those during calibration. Electrical-model-based methods include high-frequency signal injection methods for standstill and low-speed operation [12–16], [25–32], and flux observation methods for

medium- and high-speed operation [17], [33–44]. High-frequency signal injection methods estimate the magnet temperature by observing high-frequency resistance or inductance that depend on the magnet temperature. In reference [32], a maximum estimation error of 3°C was reported. Flux observation methods estimate the permanent magnet temperature by observing the magnetic flux of the permanent magnet on the basis of the PMSM voltage equations. In reference [17], an accuracy of ±4°C was reported. In these electrical-model-based methods, because the estimated temperature depends on the temperatures of all magnets, it is not possible to estimate the temperature of only an arbitrary individual magnet.

The authors have proposed a magnet temperature detection method for PMSMs using electromagnetic induction and a thermistor [45–46]. Reference [46] shows that the input power of the temperature detection circuit monotonically decreases as the thermistor temperature increases. However, changes in the characteristics of the temperature detection circuit due to variations in circuit parameters were not considered. Furthermore, the temperature-detection accuracy using the temperature detection circuit was not verified.

In this paper, variations in winding resistance caused by changes in coil temperature are considered. The thermistor resistance that reduces the influence of these variations on temperature-detection accuracy is identified. Additionally, the thermistor temperature is detected from the measured DC input power of the temperature detection circuit.

II. Magnet Temperature Detection System

A. Temperature Detection Circuit

Fig. 1 shows the temperature detection circuit. An NTC thermistor is connected as the load in the wireless power transfer (WPT) system with a series-series (S-S) compensation. The WPT system is driven by the inverter.

The resistance R_{th} of an NTC thermistor is a function of its temperature T and is given by (1) using the B constant, where R_0 is the resistance at the reference temperature T_0.

$$R_{\mathrm{th}}(T) = R_0 \exp\left\{B\left(\frac{1}{T}-\frac{1}{T_0}\right)\right\} \tag{1}$$

When the resonance condition given by (2) is satisfied, the impedance Z_1 seen from the primary side of the S-S compensation WPT system is given by (3), where ω_0 is the resonant angular frequency. Equation (3) shows the dependence of the impedance Z_1 seen from the primary side on the thermistor resistance R_{th} and the thermistor temperature T.

$$\omega_0 L_1 - \frac{1}{\omega_0 C_1} = \omega_0 L_2 - \frac{1}{\omega_0 C_2} = 0 \tag{2}$$

$$Z_1(R_{\mathrm{th}},\, T) = \frac{r_1(r_2 + R_{\mathrm{L}}) + (\omega_0 M)^2}{r_2 + R_{\mathrm{th}}(T)} \tag{3}$$

The DC input power P_{DC} to the inverter, ignoring inverter losses, is equal to the primary-side power P_1 and is given by (4). The input power P_{DC} depends on the thermistor temperature T.

$$\begin{aligned} P_{\mathrm{DC}}(R_{\mathrm{th}}, T) &\approx \mathrm{Re}\left\{\frac{\dot{V}_{1\mathrm{f}}^2}{\bar{\dot{Z}}_1(R_{\mathrm{th}}, T)}\right\} \\ &= \frac{r_2 + R_{\mathrm{th}}(T)}{r_1\{r_2 + R_{\mathrm{th}}(T)\} + (\omega_0 M)^2} V_{1\mathrm{f}}^2 \end{aligned} \tag{4}$$

There is a one-to-one relationship between the input power P_{DC} and the thermistor temperature T. Differentiating (4) with respect to the load resistance R_{th} yields (5). Equation (5) is always positive. Therefore, the primary-side power P_1 of the S-S compensated WPT system increases monotonically as the load resistance increases. Then, as the thermistor temperature T increases, the resistance R_{th} decreases, and the input power P_{DC} to the temperature detection circuit decreases monotonically. This characteristic enables the detection of the thermistor temperature based on the input power to the temperature detection circuit.

$$\frac{\partial P_{\mathrm{DC}}}{\partial R_{\mathrm{th}}(T)} \approx \frac{(\omega_0 M)^2}{\left[r_1\{r_2 + R_{\mathrm{th}}(T)\} + (\omega_0 M)^2\right]^2} V_{1\mathrm{f}}^2 > 0 \tag{5}$$

B. System Configuration

Fig. 2 shows the configuration of the proposed temperature detection system. The system comprises a stationary part and a rotating part. The stationary part consists of the power detector, the DC power supply, the inverter and the primary circuit of the temperature detection circuit. The power detector measures the DC voltage and DC current supplied from the DC power supply to the inverter and detects the DC power. Note that the inverter is provided separately from the PMSM drive circuit. The rotating part consists of the secondary circuit, including the thermistor, and rotates with the PMSM rotor. The thermistor is attached to the magnet, which is the temperature-detection target, on the rotor.

In the proposed system, the stationary and rotating parts are magnetically coupled. Therefore, the system does not suffer wear from physical contact. In addition, because power is supplied from the stationary part to the rotating part by WPT, no power source, such as a battery, is required on the rotating part. Furthermore, since only the temperature of the magnet to which the thermistor is attached is detected, the temperatures of other parts do not affect the detection.

C. Temperature Detection Method

The thermistor temperature is detected using the regression model of the input power to the temperature detection circuit, which is measured and introduced by preliminary examinations. The temperature characteristic of the input power is fitted by (6). Fig. 3 shows the block diagram

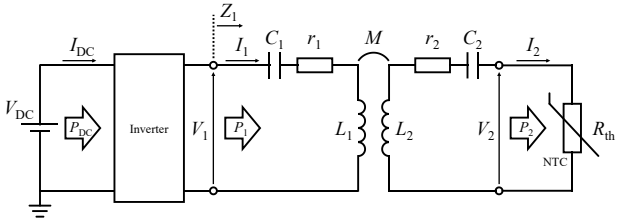

Fig. 1. Proposed temperature detection circuit.

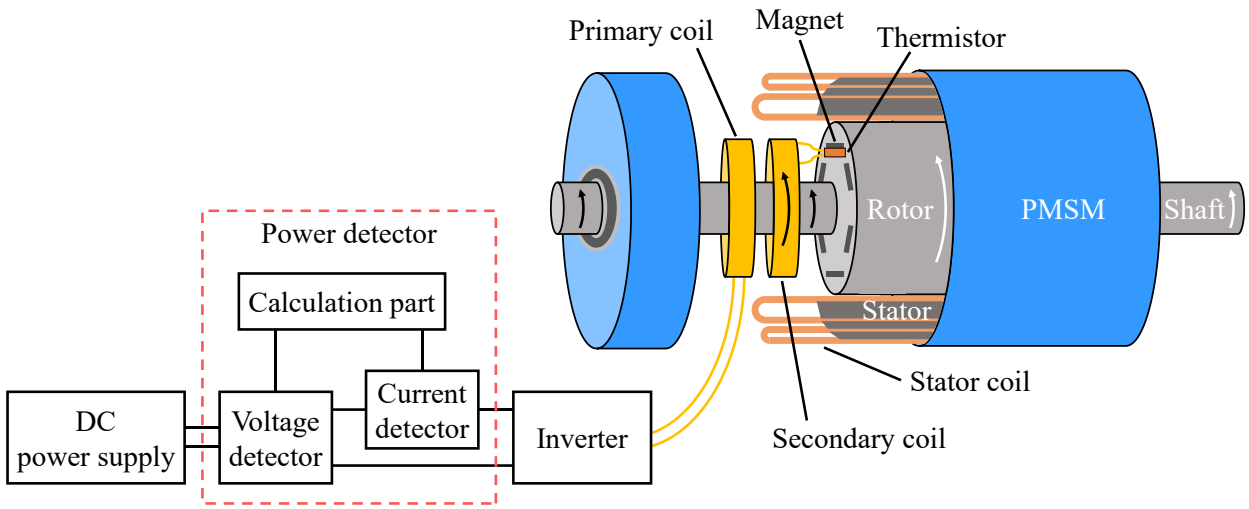

Fig. 2. Configuration of proposed temperature detection system.

of the proposed method. First, measure the DC input power P_{DC} supplied to the temperature detection circuit from the DC power supply. Next, use the measured input power P_{DC} to determine the thermistor temperature T_{dtc} according to (7). Equation (7) follows from (6). The coefficients a, b and c are experimentally determined by a preliminary experiment.

$$P_{DC} = a\exp(-bT) + c \tag{6}$$

$$T_{dtc} = \frac{1}{b}\ln\left(\frac{a}{P_{DC} - c}\right) \tag{7}$$

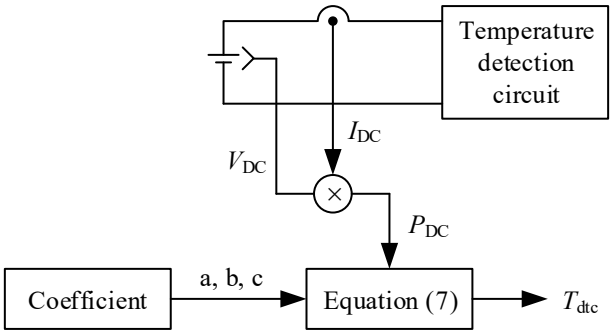

Fig. 3. Block diagram of temperature detection.

III. Thermistor Resistance for Improving Temperature-Detection Accuracy

A. Effect of Variations in Circuit Parameters

If the circuit parameters deviate from the conditions under which the input-power regression model was built, the actual input power at a specific thermistor temperature will differ from the expected input power. Variations in these parameters lead to an increase in temperature detection errors. One possible cause is variations in the winding resistance. Winding resistance depends on the winding temperature. In practice, the winding temperature varies due to copper loss in the winding and heat conduction from the motor. The resistance R of a metal at temperature T, with resistance at the reference temperature T_0, is given by (8). Here, α is the temperature coefficient, and for copper, $\alpha \approx 4.0\times10^{-3}$°C^{-1}.

$$R = R_0\{1 + \alpha(T - T_0)\} \tag{8}$$

From (3), when winding resistance $r_1 = r_2 = r$, the impedance Z_1 seen from the primary side of the WPT system is given by (9). Differentiating (9) with respect to the winding resistance r yields (10). Equation (10) represents the variation in the primary-side impedance Z_1 with respect to the winding resistance r. Equation (10) becomes zero when the condition in (11), which depends on the resonance frequency and the coil parameters, is satisfied. As the thermistor resistance R_{th} deviates further from the condition given in (11), the absolute value of (10) increases. In other words, the variation in the primary-side impedance Z_1 with respect to the winding resistance r becomes larger. As a result, the variation in the input power P_{DC} of the temperature detection circuit also increases. Therefore, the temperature detection error is expected to increase as the thermistor resistance R_{th} deviates farther from the condition given in (11). On the other hand, when the thermistor resistance R_{th} is close to the condition in (11), the primary-side impedance Z_1 and the input power P_{DC} of the temperature detection circuit are robust against variations in the winding resistance r. Consequently, the temperature detection error is reduced.

$$Z_1 = r + \frac{(\omega_0 M)^2}{r + R_{th}} \tag{9}$$

$$\frac{\partial Z_1}{\partial r} = 1 - \frac{(\omega_0 M)^2}{(r + R_{th})^2} \tag{10}$$

$$R_{th} = \omega_0 M - r \tag{11}$$

B. Simulation

The effect of variations in winding resistance on the accuracy of temperature detection was investigated using a simulation. Table 1 shows the parameters for the simulation.

The thermistor resistance satisfying the condition of (11) is R_{th} = 1.29 Ω. According to (8), a copper winding with a resistance of 100 mΩ at room temperature (assumed here to be 25°C) has a resistance of 150 mΩ at 150°C. In this study, simulations were conducted for thermistors whose resistances at 25°C were 1, 10, and 20 Ω. The B-constant was 2750 K for all thermistors. First, the temperature characteristic model of the input power was built for each thermistor based on the method described in the previous chapter. Next, the thermistor resistance was fixed at values corresponding to 50°C, 100°C, and 150°C, while the winding resistances r_1 and r_2 were varied from 100 mΩ to 150 mΩ in steps of 10 mΩ. For each condition, the thermistor temperature T_{dtc} was then calculated from the input power using the temperature characteristic model.

Fig. 4 shows the simulation results. The results for thermistors with resistances of 1, 10, and 20 Ω at 25°C are shown by the circles, squares, and triangles plots, respectively. In Fig. 4 (a), (b) and (c), the thermistor temperature are assumed to be 50°C, 100°C and 150°C, respectively. The legend shows the thermistor resistance at each temperature. The results indicate that as the winding resistance increases relative to the conditions used to develop the regression model, the temperature detection error also increases. The results also show that the closer the thermistor resistance is to the conditions in (7), the smaller the temperature detection error. At 50°C, the best temperature-detection accuracy is achieved with a thermistor whose resistance is 1 Ω at 25°C. From these results, it is confirmed that as the thermistor resistance approaches the condition in (7), the input power of the temperature detection circuit becomes more robust to variations in winding resistance, and the temperature detection error is reduced.

IV. Temperature Detection Experiments

A. Prototype System

In the previous section, a design method for thermistor resistance was presented that can reduce the influence of variations in winding resistance on temperature-detection accuracy. This section describes experiments conducted with a prototype system that employs a thermistor (BN-LG25Y1R0MYB) with a resistance of 1 Ω at 25°C. The characteristics of the thermistor are as follows: The B constant (25°C/85°C) is B = 2750K. The rated power is 7 W. The rated current is 15 A at ambient temperatures between 0°C and 25°C, and it decreases linearly above 25°C, reaching 0 A at 200°C.

TABLE I. Parameters for Simulation.

Parameter	Symbol	Value
DC input voltage	V_{DC}	3 V
Resonant frequency	f	100 kHz
Coil inductance	L_1, L_2	7.4 μH
Coil windng resistance @ 25°C	r_1, r_2	100 mΩ
Resonant capacitor	C_1, C_2	342 nF
Coupling coefficient	k	0.3
Mutual inductance	M	2.22 μH

Table 2 shows the designed circuit parameters. The DC input voltage V_{DC} was determined to ensure that the secondary-side current I_2 and secondary-side power P_2 do not exceed the rated values of the thermistor. The value of secondary-side capacitor C_2 was determined considering the inductance of the cable connecting the WPT system to the thermistor in the thermostatic chamber. The cable is long, with an inductance of 1.15 μH, which is large compared to the inductances of the primary- and secondary-side coils.

The experimental setup was configured as follows. A solenoid coil with a diameter of 75 mm, a length of 3.2 mm and 6 turns is used for both the primary-side and secondary-

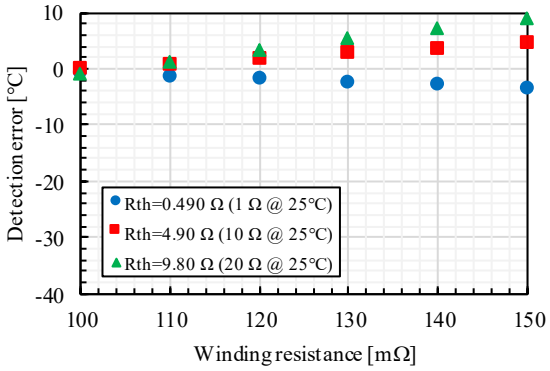

(a)

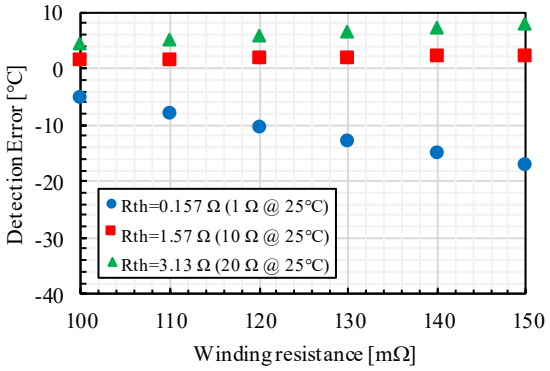

(b)

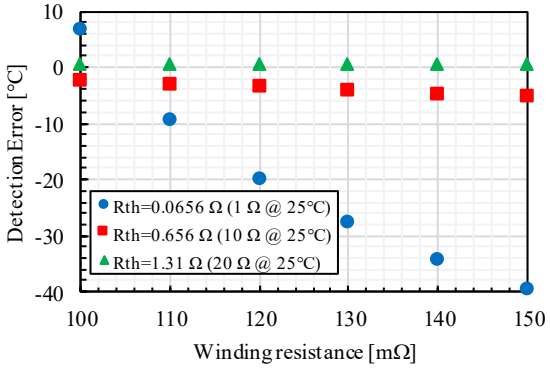

(c)

Fig. 4. Temperature detection error caused by variations in winding resistance. (a) T = 50°C. (b) T = 100°C. (c) T = 150°C

side. The coils were placed 11.5 mm apart. The coils are intended to be attached around the shaft of a PMSM. However, the experiment in this paper was conducted without attaching the coils around the shaft in order to simplify the experimental setup and to neglect the effects of iron losses. Furthermore, the secondary-side circuit corresponding to the rotating part was not rotated. Only the thermistor was placed in the thermostatic chamber, and the temperature was varied. The thermocouple attached to the thermistor measured its actual temperature.

B. Temperature Characteristic of Input Power

Fig. 5 shows the input power of the prototype temperature detection circuit. The measured values are fitted by (6). The coefficients of the regression curve are $a = 4.77$, $b = 0.0259$, $c = 1.26$. The regression curve of the input power P_{DC} decreases monotonically as the thermistor temperature T increases. This equals the theoretical characteristic. This characteristic ensures that the thermistor temperature is uniquely determined from the measured DC power.

C. Temperature-Detection Accuracy

The temperature-detection accuracy of the proposed method has been verified. The thermistor temperature was varied by a thermostatic chamber to simulate the heating during operation and cooling during shutdown of a PMSM. Fig. 6 shows the experimental results. Fig. 6 (a) indicates that the input power P_{DC} decreases as the thermistor temperature T increases, and P_{DC} increases as T falls. This result is consistent with the input power characteristics shown in the previous section. Fig. 6 (b) shows the temperature T_{dtc} detected by (7) and the detection error. The detected temperature T_{dtc} varies in accordance with the actual thermistor temperature T. The proposed method achieves temperature detection with an accuracy of ±4°C.

TABLE II. PARAMETERS FOR PROTOTYPE SYSTEM.

Parameter	Symbol	Value
DC input voltage	V_{DC}	5 V
Resonant frequency	f	100 kHz
Primary coil inductance	L_1	7.4 μH
Secondary coil inductance	L_2	7.4 μH
Primary coil windng resistance	r_1	120 mΩ
Secondary coil windng resistance	r_2	130 mΩ
Primary resonant capacitor	C_1	341 nF
Secondary resonant capacitor	C_2	285 nF
Coupling coefficient	k	0.293
Mutual inductance	M	2.17 μH

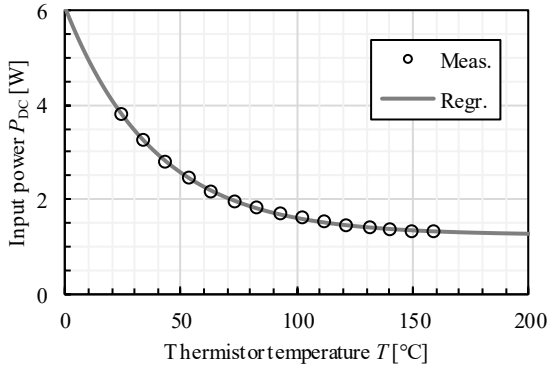

Fig. 5. Input power variation with thermistor temperature.

V. CONCLUSION

This paper proposed a magnet temperature detection method for PMSMs using a WPT system and an NTC thermistor, and verified its temperature-detection accuracy and robustness to variations in circuit parameters. First, the principle of the proposed method was clarified theoretically. It was shown that the DC input power of the temperature detection circuit varies monotonically with the thermistor resistance and, therefore, with the thermistor temperature. This one-to-one relationship enables thermistor temperature detection from the measured DC input power. Next, the effect of variations in winding resistance on temperature-detection accuracy was analyzed. The analysis showed that the

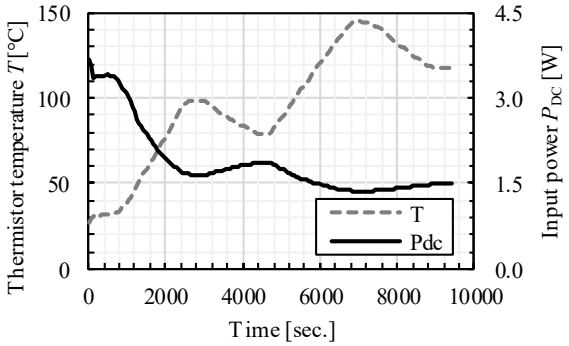

(a)

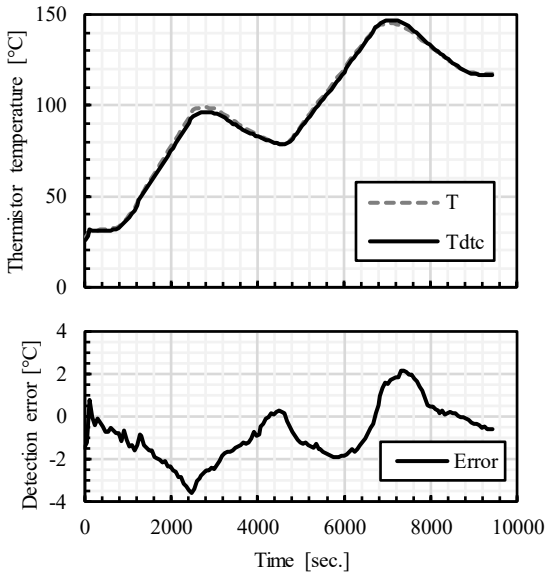

(b)

Fig. 6. Tempetarure detection results. (a) Time variation in input power of temperature detection circuit. (b) Detected temperature and detection error.

sensitivity of the primary-side impedance to winding resistance depends on the thermistor resistance and becomes zero under the derived condition. Simulation results demonstrated that the temperature detection error decreases when the thermistor resistance is selected to be close to this condition. Finally, a prototype system was constructed, and its input-power characteristic and temperature-detection accuracy were experimentally evaluated. The experimental results confirmed that the input power decreases monotonically as the thermistor temperature increases, in agreement with the theoretical analysis, and that the proposed method achieved a detection accuracy of ±4°C. These results confirm the validity of the proposed detection principle and provide a useful design guideline for selecting thermistor resistance to improve robustness to variations in winding resistance.

REFERENCES

[1] H. Toda, Z. Xia, J Wang, K. Atallah, and D. Howe, "Rotor Eddy-Current Loss in Permanent Magnet Brushless Machines," IEEE Trans. on Magn., vol. 40, no. 4, pp. 2104–2106, 2004.

[2] K. Yamazaki and A. Abe, "Loss Investigation of Interior Permanent-Magnet Motors Considering Carrier Harmonics and Magnet Eddy Currents ," IEEE Trans. on Ind. Appl., vol. 45, no. 2, pp. 659–665, 2009.

[3] N. Zhao, Z. Q. Zhu, and W. Liu, "Rotor Eddy Current Loss Calculation and Thermal Analysis of Permanent Magnet Motor and Generator," IEEE Trans. on Magn., vol. 47, no. 10, pp. 4199–4202, 2011.

[4] M. D. Calin and E. Helerea, "Temperature Influence on Magnetic Characteristics of NdFeB Permanent Magnets," in Proc. 7th Int. Symp. Adv. Topics Electr. Eng. (ATEE), pp. 1–6, 2011.

[5] S. Li, B. Sarlioglu, S. Jurkovic, N. R. Patel, and P. Savagian, "Analysis of Temperature Effects on Performance of Interior Permanent Magnet Machines for High Variable Temperature Applications," IEEE Trans. on Ind. Appl., vol. 53, no. 5, pp. 4293–4933, 2017.

[6] S. Li, B. Sarlioglu, S. Jurkovic, N. R. Patel, and P. Savagian, "Comparative Analysis of Torque Compensation Control Algorithms of Interior Permanent Magnet Machines for Automotive Applications Considering the Effects of Temperature Variation," IEEE Trans. on Transport. Electrific., vol. 3, no. 3, pp. 668–681, 2017.

[7] K. Matsuoka, M. Kondo, and Y. Shimizu, "Totally-Enclosed Type Traction Motor Using Permanent Magnet Synchronous Motor," IEEJ Trans. IA, vol. 124, no. 2, 2004.

[8] M. Ganchev, H. Umschaden, and H. Kappeler, "Rotor temperature distribution measuring system," in Proc. IECON 2011 - 37th Annu. Conf. IEEE Ind. Electron. Soc., pp.2006–2011, 2011.

[9] D. Fernandez, D. Reigosa, T. Tanimoto, T. Kato, and F. Brizm "Wireless permanent magnet temperature & field distribution measurement system for IPMSMs," in Proc. IEEE Energy Convers. Congr. Expo. (ECCE), pp.3996–4003, 2015.

[10] D. Park, H. S. Jung, H. J. Cho, and S. K. Sul, "Design of Wireless Temperature Monitoring System for Measurement of Magnet Temperature of IPMSM," in Proc. IEEE Transportation Electrification Conf. Expo. (ITEC), pp. 656–661, 2018.

[11] J. Feng, D. Liang, Z. Q. Zhu, S. Guo, Y. Li, and A. Zhao, "Improved Low-Order Thermal Model for Critical Temperature Estimation of PMSM," IEEE Trans. on Energy Convers., vol. 37, no. 1, pp. 413–423, 2022.

[12] D. D. Reigosa, F. Briz, P. García, J. M. Guerrero, and M. W. Degner, "Magnet Temperature Estimation in Surface PM Machines Using High-Frequency Signal Injection," IEEE Trans. on Ind. Appl., vol. 46, no. 4, pp. 1468–1475, 2010.

[13] D. D. Reigosa, D. Fernandez, H. Yoshida, T. Kato, and F. Briz, "Permanent-Magnet Temperature Estimation in PMSMs Using Pulsating High-Frequency Current Injection," IEEE Trans. on Ind. Appl., vol. 51, no. 4, pp. 3159–3168, 2015.

[14] G. Feng, C. Lai, and N. C. Kar, "Expectation-Maximization Particle-Filter- and Kalman-Filter-Based Permanent Magnet Temperature Estimation for PMSM Condition Monitoring Using High-Frequency Signal Injection," IEEE Trans. on Ind. Informat., vol. 13, no. 3, pp. 1261–1270, 2017.

[15] G. Feng, C. Lai, K. L. V. Iyer, and N. C. Kar, "Improved High-Frequency Voltage Injection Based Permanent Magnet Temperature Estimation for PMSM Condition Monitoring for EV Applications," IEEE Trans. on Veh. Technol. , vol. 67, no. 1, pp. 216–225, 2018.

[16] A. Ito, K. Ohishi, Y. Yokokura, Y. Ide, D. Kuraishi, A. Takahashi, and M. Kitahara, "Simultaneous temperature estimation of winding and magnet of pmsm by high-frequency-injection into static coordinate," IEEJ The Papers of Joint Technical Meeting on "Semiconductor Power Converter" and "Motor Drive", SPC-22-166/MD-22-101, pp.127–132, September 2022.

[17] B. Wen, K. Liu, Z. Q. Zhu, and R. Ding, "Estimation of Magnet Temperature for Integer-Slot PMSMs via Extraction of First-Order Slot Harmonic in Back EMF," IEEE Trans. Transport. Electrific., vol. 10, no. 3, pp. 7203–7213, 2024.

[18] M. Kamiya, H. Awata, T. Miura, Y. Yagyu, T. Kosaka, and N. Matsui, "Permanent magnet temperature analysis considering pwm carrier harmonics for interior permanent magnet synchronous generator in hybrid vehicles," IEEJ Trans. IA, vol. 127, no. 12, pp.1238–1244, 2007.

[19] G. D. Demetriades, H. Z. de la Parra, E. Andersson, and H. Olsson, "A Real-Time Thermal Model of a Permanent-Magnet Synchronous Motor," IEEE Trans. Power Electron. , vol. 25, no. 2, pp. 463–474, 2010.

[20] B. H. Lee, K. S. Kim, J. W. Jung, J. P. Hong, and Y. K. Kim, "Temperature Estimation of IPMSM Using Thermal Equivalent Circuit," IEEE Trans. on Magn., vol. 48, no. 11, pp. 2949–2952, 2012.

[21] T. Huber, W. Peters, and J. Böcker, "Monitoring critical temperatures in permanent magnet synchronous motors using low-order thermal models," in Proc. Int. Power Electron. Conf. (IPEC-Hiroshima 2014 - ECCE ASIA), pp. 1508–1515, 2014.

[22] C. Kral, A. Haumer, and S. B. Lee, "A Practical Thermal Model for the Estimation of Permanent Magnet and Stator Winding Temperatures," IEEE Trans. Power Electron. , vol. 29, no. 1, pp. 455–464, 2014.

[23] Y. Imanishi and S. Nishiguchi, "Development of temperature estimation for motor magnet of electric vehicle," SAEJ Trans., vol. 45, no. 5, pp.841–845, September 2014.

[24] O. Wallscheid and J. Böcker, "Global Identification of a Low-Order Lumped-Parameter Thermal Network for Permanent Magnet Synchronous Motors," IEEE Trans. on Energy Convers., vol. 31, no. 1, pp. 354–365, 2016.

[25] M. Ganchev, C. Kral, and T. Wolbank, "Sensitivity and robustness aspects of sensorless rotor temperature estimation technique for Permanent Magnet Synchronous Motor," in Proc. 15th Int. Power Electron. Motion Control Conf. (EPE/PEMC), pp. LS3a-1.2-1– LS3a-1.2-6, 2012.

[26] M. Ganchev, C. Kral, and T. Wolbank, "Sensorless rotor temperature estimation of permanent magnet synchronous motor under load conditions," in Proc. IECON 2012 - 38th Annu. Conf. IEEE Ind. Electron. Soc., pp. 1999–2004, 2012.

[27] D. Fernandez, M. Martínez, D. D. Reigosa, J. M. Guerrero, C. M. S. Alvarez, and F. Briz, "Influence of Magnetoresistance and Temperature on Permanent Magnet Condition Estimation Methods Using High-Frequency Signal Injection," IEEE Trans. on Ind. Appl., vol. 54, no. 5, pp. 4218–4226, 2018.

[28] D. Reigosa, D. Fernández, M. Martínez, J. M. Guerrero, A. B. Diez, and F. Briz, "Magnet Temperature Estimation in Permanent Magnet Synchronous Machines Using the High Frequency Inductance," in Proc. IEEE Energy Convers. Congr. Expo. (ECCE), pp.5029–5034, 2018.

[29] H. S. Jung, D. Park, H. Kim, S. K. Sul, and D. J. Berry, "Non-Invasive Magnet Temperature Estimation in IPMSM by High Frequency Pulsating Sinusoidal Voltage Injection," in Proc. IEEE Transportation Electrification Conf. Expo. (ITEC), pp.858–862, 2018.

[30] H. S. Jung, D. Park, H. Kim, S. K. Sul, and D. J. Berry, "Non-Invasive Magnet Temperature Estimation of IPMSM Based on High-Frequency Inductance With a Pulsating High-Frequency Voltage Signal Injection," IEEE Trans. on Ind. Appl., vol. 55, no. 3, pp. 3076–3086, 2019.

[31] H. S. Jung, H. Kim, S. K. Sul, and D. J. Berry, "Magnet Temperature Estimation of Traction Motor in Standstill With Considering Spatial Harmonics," IEEE Trans. Ind. Electron., vol. 68, no. 11, pp. 10546–10557, 2021.

[32] H. Kim, H. S. Jung, and S. K. Sul, "Stator Winding Temperature and Magnet Temperature Estimation of IPMSM Based on High-Frequency

Voltage Signal Injection," IEEE Trans. Ind. Electron., vol. 70, no. 3, pp. 2296–2306, 2023.

[33] A. Specht and J. Böcker, "Observer for the rotor temperature of IPMSM," in Proc. 14th Int. Power Electron. Motion Control Conf. (EPE-PEMC 2010), pp. T4-12– T4-15, 2010.

[34] A. Specht, O. Wallscheid, and J. Böcker, "Determination of rotor temperature for an interior permanent magnet synchronous machine using a precise flux observer," in Proc. Int. Power Electron. Conf. (IPEC-Hiroshima 2014 - ECCE ASIA), pp. 1501–1507, 2014.

[35] K. Liu and Z. Q. Zhu, "Online Estimation of the Rotor Flux Linkage and Voltage-Source Inverter Nonlinearity in Permanent Magnet Synchronous Machine Drives," IEEE Trans. Power Electron., vol. 29, no. 1, pp. 418–427, 2014.

[36] G. Feng, C. Lai, K. Mukherjee, and N. C. Kar, "Current Injection-Based Online Parameter and VSI Nonlinearity Estimation for PMSM Drives Using Current and Voltage DC Components," IEEE Trans. Transport. Electrific., vol. 2, no. 2, pp. 119–128, 2016.

[37] O. Wallscheid, A. Specht, and J. Böcker : "Observing the Permanent-Magnet Temperature of Synchronous Motors Based on Electrical Fundamental Wave Model Quantities," IEEE Trans. Ind. Electron., vol. 64, no. 5, pp. 3921–3929, 2021.

[38] G. Feng, C. Lai, J. Tjong, and N. C. Kar, "Noninvasive Kalman Filter Based Permanent Magnet Temperature Estimation for Permanent Magnet Synchronous Machines," IEEE Trans. Power Electron., vol. 33, no. 12, pp. 10673–10682, 2018.

[39] H. S. Jung, H. Kim, S. K. Sul, and D. J. Berry, "Magnet Temperature Estimation of IPMSM by Using Reactive Energy," in Proc. 10th Int. Conf. Power Electron. ECCE Asia (ICPE 2019 - ECCE Asia), pp. 582–587, 2019.

[40] T. Kato, K. Sasaki, D. F. Laborda, D. F. Alonso, and D. D. Reigosa, "Magnet Temperature Estimation Methodology by Using Magnet Flux Linkage Observer for Variable Leakage Flux IPMSM," IEEJ Trans. IA, vol. 140, no. 4, 2020.

[41] H. S. Jung, H. Kim, S. K. Sul, and D. J. Berry, "Temperature Estimation of IPMSM by Using Fundamental Reactive Energy Considering Variation of Inductances," IEEE Trans. Power Electron., vol. 36, no. 5, pp. 5771–5783, 2021.

[42] H. S. Jung, H. Kim, S. K. Sul, and D. J. Berry, "Permanent Magnet Temperature Estimation in a Mass-Produced Traction Motor for an Electric Vehicle," IEEE Trans. Transport. Electrific., vol. 8, no. 2, pp. 1863–1873, 2022.

[43] H. S. Jung and D. Y. Oh, "Estimation of Stator and Magnet Temperatures of IPMSM From Active and Reactive Energies at Medium and High Speeds," IEEE Trans. Transport. Electrific., vol. 9, no. 2, pp. 2983–2993, 2023.

[44] S. Arai, R. Akaki, R. Miyano, "Error Reduction in Estimating Magnet Temperature of Interior Permanent Magnet Synchronous Motor Using Induced Voltage," IEEJ Trans. IA, vol. 145, no. 8, 2025.

[45] Y. Hojo, "Temperature detection system," Patant No. 7201462, 2019.

[46] R. Hamba, K. Kusaka, Y. Hojo, "Magnet Temperature Detection of PMSM with Wireless Power Transfer," in Proc. 13th Int. Conf. Renewable Energy Res. Appl. (ICRERA), pp. 1068–1073, 2024.